This is a repository copy of *Current-limiting three-phase rectifiers*.

White Rose Research Online URL for this paper:
http://eprints.whiterose.ac.uk/114856/

Version: Accepted Version

Article:
Zhong, Q.-C. and Konstantopoulos, G.C. orcid.org/0000-0003-3339-6921 (2018) Current-limiting three-phase rectifiers. IEEE Transactions on Industrial Electronics, 65 (2). pp. 957-967. ISSN 0278-0046

https://doi.org/10.1109/TIE.2017.2696483

© 2017 IEEE. Personal use of this material is permitted. Permission from IEEE must be obtained for all other users, including reprinting/ republishing this material for advertising or promotional purposes, creating new collective works for resale or redistribution to servers or lists, or reuse of any copyrighted components of this work in other works. Reproduced in accordance with the publisher's self-archiving policy.

Reuse
Items deposited in White Rose Research Online are protected by copyright, with all rights reserved unless indicated otherwise. They may be downloaded and/or printed for private study, or other acts as permitted by national copyright laws. The publisher or other rights holders may allow further reproduction and re-use of the full text version. This is indicated by the licence information on the White Rose Research Online record for the item.

Takedown
If you consider content in White Rose Research Online to be in breach of UK law, please notify us by emailing eprints@whiterose.ac.uk including the URL of the record and the reason for the withdrawal request.

eprints@whiterose.ac.uk
https://eprints.whiterose.ac.uk/

Current-limiting Three-phase Rectifiers

Qing-Chang Zhong, *Fellow*, *IEEE*, and George C. Konstantopoulos, *Member*, *IEEE*

***Abstract*—In this paper, a nonlinear controller is proposed for a three-phase rectifier so that its input current does not exceed a given limit. At the same time, the proposed controller can achieve accurate dc output voltage regulation and reactive power control independently from system parameters including the load during the normal operation. Using the generic dq transformation and the nonlinear model of the rectifier, the boundedness and the current-limiting property of the closed-loop system are proven using Lyapunov methods and the input-to-state stability theory. Moreover, an analytic framework for selecting the controller parameters is presented and the current limitation is proven for both the cases with L and LCL filters at the input of the rectifier. Different from existing approaches, the current-limiting property is achieved without external limiters, monitoring devices or switches and is incorporated in the control dynamics, independently from the type of the load (linear or nonlinear). Extensive real-time simulation results are provided to verify the effectiveness of the proposed strategy.**

***Index Terms*—Three-phase rectifier, nonlinear control, current-limiting property, stability.**

I. Introduction

THE AC/DC power converters are widely used in the integration of renewable energy systems, energy storage systems, and loads to the smart grid [1]–[3]. Single-phase or three-phase power converters are usually controlled using pulse-width-modulated (PWM) methods to achieve accurate dc bus voltage regulation, power factor correction, bi-directional power flow and low harmonic distortion of the grid current [4], [5].

Particularly for three-phase rectifiers, various control techniques have been proposed to achieve dc output voltage regulation and unity power factor operation. Although in most applications, the unity power factor is expected, modern control technologies for rectifiers dictate a need for flexibility in controlling the reactive power, especially in microgrid and smart-grid applications [1], [6]. Using the voltage-oriented control approach and the Park transformation, traditional control methods have been designed to include a single Proportional-Integral (PI) controller for achieving the desired unity power factor and a cascaded PI controller for regulating the dc output voltage [7]–[10]. The inner loop is often replaced with hysteresis controllers, especially in virtual-flux-based control methods [11], [12], while intelligent control methods have been also proposed to improve the rectifier's performance [13], [14]. Recently, direct power control has been applied to three-phase rectifiers which is based on a predefined look-up table, but apart from its simple structure, it often produces high power ripples and introduces a variable switching frequency [15], [16]. Although traditional control methods may result in a stable system using small-signal modeling or by considering several assumptions [17], [18], most of the above methods lack of rigorous nonlinear stability proof for the closed-loop system, which is of major importance in smart grids. Since the three-phase rectifiers are inherently nonlinear systems, the nonlinear closed-loop stability is often difficult to prove.

Based on the nonlinear dynamic model of the rectifier, passivity-based [19], [20] and advanced nonlinear controllers, mainly based on feedback linearization [21]–[23], have been proposed to guarantee asymptotic performance. However, the resulting control scheme is often complicated, difficult to implement and depends on most of the system parameters, thus reducing the applicability of these methods in practice. Moreover, the stability of three-phase rectifiers should also consider the physical limitations of the converter. For example, the grid current and consequently the dc output voltage should be maintained below some given values, since external disturbances or undesired oscillations during transients can be catastrophic for converters [24], [25]. Although some nonlinear controllers with a proven stability bound have been designed [26], [27], a given limit for the grid current below a specific value is still not guaranteed. The current-limiting property is crucial to maintain a stable and reliable operation of rectifiers during transients, since high currents can damage the device and the load. A current-limiting method for single-phase rectifiers or inverters has been recently reported in [28], [29], but the concept cannot be directly extended to three-phase rectifiers using the dq modeling, mainly due to the coupling between the d and q components and the different model description. Although the traditional control methods based on single and cascaded control can be equipped with additional limiters and saturation units to achieve a current-limiting function, they suffer from integrator windup and instability [30], [31]. These approaches require anti-windup techniques which further complicate the system and consequently the stability analysis. Particularly, traditional anti-windup methods lack of a rigorous stability analysis, while modern anti-windup techniques require knowledge of the system parameters [32],

Manuscript received November 1, 2016; revised January 21, 2017 and March 10, 2017; accepted April 3, 2017. This work was supported by the EPSRC under Grant No. EP/J01558X/1.

Q.-C. Zhong is with the Department of Electrical and Computer Engineering, Illinois Institute of Technology, Chicago, IL 60616, USA, and was with the Department of Automatic Control and Systems Engineering, The University of Sheffield, Sheffield, S1 3JD, UK (e-mail: zhongqc@ieee.org).

G. C. Konstantopoulos is with the Department of Automatic Control and Systems Engineering, The University of Sheffield, Sheffield, S1 3JD, UK (e-mail: g.konstantopoulos@sheffield.ac.uk).

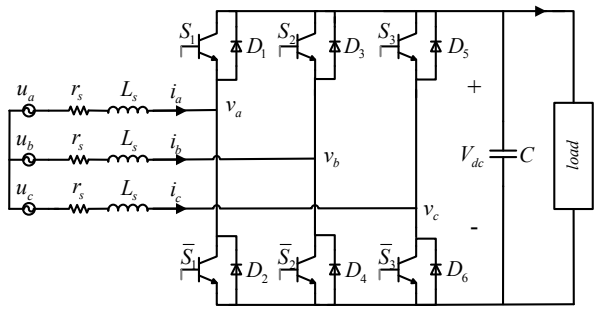

Fig. 1. The three-phase rectifier under investigation

[33]. In addition, traditional current-limiting approaches apply the saturation unit at the output of the outer loop which guarantees a limit for the reference value of the current but not for the transient response. The main goal of this paper is to design a controller for a three-phase rectifier that maintains the grid current below a given limit at all times (even during transients), achieves dc output voltage regulation and power factor control, acts independently from system parameters, and guarantees nonlinear closed-loop stability.

To this end, the generic nonlinear dynamic model of the three-phase rectifier is firstly obtained. Initially, a resistive load is considered at the output of the rectifier for simplicity, but later the results are extended to power converter-fed loads which are commonly found in a smart grid. Although almost in all applications the axis α of the stationary frame is oriented with the phase a of the grid voltage [1], in this paper, the generic $\alpha\beta$ transformation is used, which offers a significant advantage in the proposed control design. Based on the generic synchronously rotating dq nonlinear model of the converter, a parameter-free current-limiting nonlinear controller is proposed and analyzed with the Lyapunov methods, motivated by the recently proposed bounded integral controller in [34]. It introduces bounded dynamic virtual resistances in the dq dynamics of the input current, which leads to a current limited by a given maximum value for the three-phase rectifier. The current-limiting property of the controller is independent of the filter inductor, the dc capacitor and the load. Using the input-to-state stability theory [35], it is analytically proven that the closed-loop dq current responses are bounded and the root-mean-square (RMS) value of the input current is always kept below a given limit. The current limitation is achieved without removing the coupling terms in the dq current dynamics. This operation is achieved without additional switches or monitoring devices and the proposed controller remains a continuous-time dynamical system that facilitates the stability analysis. Since modern power networks require a flexibility in controlling the reactive power and not necessarily achieve unity power factor [1], the proposed controller is proven to guarantee accurate reactive power regulation as well. The case with an LCL filter is also investigated and the proposed controller is slightly modified to guarantee that even in this case, the input current remains limited and the closed-loop system remains stable. Extensive real-time simulation results are provided to verify the effectiveness of the proposed method under changes of the load and the reactive power for both a resistive load and a power converter-fed load.

Overall, the proposed controller introduces significant differences compared to existing current-limiting strategies. Traditional current-limiting controllers which consist of a saturation unit in the reference of the inner current controller result in the following: i) only the reference current is limited, which means that the actual current can violate the limit during a transient, ii) saturation can lead to integrator windup for the outer loop controller (voltage or power controller) and consequently to continuous oscillations and instability [30], [31]. The proposed controller does not require a saturation unit, current-limitation is guaranteed using nonlinear stability theory which leads to a limit of the current during transients and it does not suffer from integrator windup or instability.

II. System Modeling

The system under consideration is a three-phase rectifier, as shown in Fig. 1. Initially a resistive load R_L is considered at the output of the rectifier but later the analysis is extended to more complicated power converter-fed loads. The rectifier consists of a boosting inductor L_s with a small parasitic resistance r_s in series for each phase, a dc output capacitor C and 6 controllable switching elements which are capable of conducting current and power in both directions and operate using PWM. The input voltages and currents of the rectifier are expressed as v_i and i_i, $i = a, b, c$, respectively, while the output dc voltage is denoted as V_{dc}. The rectifier is supplied by a three-phase balanced grid with

$$\begin{aligned} u_a &= \sqrt{2}U_{rms}\cos\theta \\ u_b &= \sqrt{2}U_{rms}\cos\left(\theta - 120^o\right) \\ u_c &= \sqrt{2}U_{rms}\cos\left(\theta + 120^o\right), \end{aligned}$$

where U_{rms} is the RMS grid voltage and $\theta = \omega t$, with ω being the grid frequency.

In order to obtain the dynamic model of the system, the average system analysis [19] and the dq transformation [1] can be used for the three-phase voltages and currents. Here, the generic $\alpha\beta$ transformation [36] with

$$T_{\alpha\beta} = \frac{2}{3}\begin{bmatrix} \cos\theta_\alpha & \cos\left(\theta_\alpha - 120^o\right) & \cos\left(\theta_\alpha + 120^o\right) \\ \sin\theta_\alpha & \sin\left(\theta_\alpha - 120^o\right) & \sin\left(\theta_\alpha + 120^o\right) \\ 0.5 & 0.5 & 0.5 \end{bmatrix}$$

is firstly applied to transform the 3-phase abc frame to the stationary $\alpha\beta$ frame, where θ_α is the angle between the a and α axes. Then, the $\alpha\beta$ frame is transformed to the synchronously rotating dq frame using the rotating transformation with

$$T_{dq} = \begin{bmatrix} \cos\theta_g & -\sin\theta_g \\ \sin\theta_g & \cos\theta_g \end{bmatrix},$$

where θ_g denotes the angle between the α and d axes, as shown in Fig. 2. Note that in Fig. 2, all the angles θ, θ_g and θ_α are calculated clockwise. Therefore, the d and q components of the grid voltages are

$$\begin{aligned} U_d &= \sqrt{2}U_{rms}\cos\left(\theta_g - (\theta - \theta_\alpha)\right) \\ U_q &= \sqrt{2}U_{rms}\sin\left(\theta_g - (\theta - \theta_\alpha)\right). \end{aligned}$$

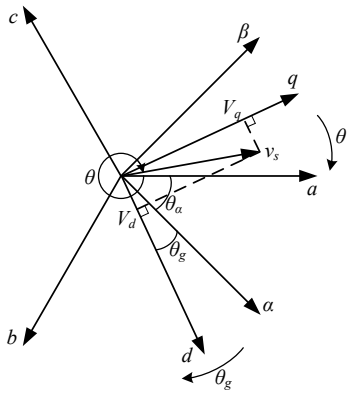

Fig. 2. Reference frames for three-phase abc systems

Since θ_g and θ synchronously change at the same speed, the difference $\theta_g - \theta$ is constant and if $\theta_g - \theta = 0$, then

$$U_d = \sqrt{2}U_{rms}\cos(\theta_\alpha) \tag{1}$$
$$U_q = \sqrt{2}U_{rms}\sin(\theta_\alpha). \tag{2}$$

In most applications, the α axis is aligned with the a axis [1], i.e., $\theta_\alpha = 0$, which results in $U_d = \sqrt{2}U_{rms}$ and $U_q = 0$. However, in this paper, the generic transformation is considered, which is shown in the sequel to be necessary for the proposed control scheme.

Following [19], the dynamic model of the rectifier in the synchronously rotating dq frame can then be found as

$$\begin{aligned} L_s\frac{dI_d}{dt} &= -r_sI_d - \omega L_sI_q - m_d\frac{V_{dc}}{2} + U_d \\ L_s\frac{dI_q}{dt} &= -r_sI_q + \omega L_sI_d - m_q\frac{V_{dc}}{2} + U_q \\ C\frac{dV_{dc}}{dt} &= \frac{3}{4}m_dI_d + \frac{3}{4}m_qI_q - \frac{V_{dc}}{R_L}, \end{aligned} \tag{3}$$

where U_d, U_q and I_d, I_q are the d and q components of the grid voltages and input currents, respectively, and

$$m_d = \frac{2V_d}{V_{dc}},\ m_q = \frac{2V_q}{V_{dc}}$$

are the duty-ratio control inputs with V_d and V_q being the d and q components of the rectifier voltage $v = \begin{bmatrix} v_a & v_b & v_c \end{bmatrix}^T$, respectively. The dynamic model of the three-phase rectifier is obviously nonlinear due to the multiplication of the control inputs with the system states, which increases the difficulty in the control design and the stability analysis. For a balanced and stiff grid, U_d and U_q are constant with values depending on the angle θ_α of the transformation $T_{\alpha\beta}$, as shown in (1)-(2).

Using the d- and q-quantities, the real and reactive power drawn by the rectifier are

$$P = \frac{3}{2}(U_dI_d + U_qI_q),\ Q = \frac{3}{2}(U_dI_q - U_qI_d). \tag{4}$$

When $\theta_\alpha = 0$, $U_d = \sqrt{2}U_{rms}$ and $U_q = 0$. Then for unity power factor operation, i.e. $Q = 0$, the current I_q should be controlled to be zero [19]. However, for a generic voltage orientation, the reactive power control should be achieved using the generic expression (4).

III. The Proposed Nonlinear Controller

A. Controller design

The basic idea of the proposed nonlinear controller is to operate the rectifier as a system with variable virtual resistances w_d and w_q in the d- and q-axes, respectively, that change dynamically within given ranges. To this end, the control signals, i.e. the duty-ratio control inputs m_d and m_q of the rectifier, are designed as

$$m_d = \frac{2}{V_{dc}}\left(\gamma(w_d)\left(w_dI_d - U_d\right) + U_d\right) \tag{5}$$
$$m_q = \frac{2}{V_{dc}}\left(\gamma(w_d)\left(w_qI_q - U_q\right) + U_q\right), \tag{6}$$

with positive constants w_{max} and w_{min}, and $\gamma(w_d) = \frac{w_{max}-w_d}{w_{max}-w_{min}} \in [0,\,1]$. The virtual resistance w_d is responsible for the regulation of the output voltage V_{dc} to a reference value V_{dc}^{ref} and the virtual resistance w_q is responsible for the regulation of the reactive power Q to the desired value Q^{ref}. However, both virtual resistances should be bounded in a given set to guarantee the stability of the closed-loop system and the current-limiting property, independently from the values of V_{dc} or Q. Note that Q is an expression of the system states, which further complicates the analysis and the desired property for w_d and w_q. Motivated by the bounded integral control structure recently proposed in [34], in order to avoid using saturation units that often lead to integrator windup and instability, the proposed control dynamics adopts the virtual resistances w_d and w_q that are designed to satisfy

$$\dot{w}_d = c_d\left(V_{dc} - V_{dc}^{ref}\right)w_{dq}^2 \tag{7}$$
$$\dot{w}_{dq} = -\frac{c_dw_{dq}}{\Delta w_m^2}\left(V_{dc}-V_{dc}^{ref}\right)(w_d-w_m) - k\left(\frac{(w_d-w_m)^2}{\Delta w_m^2} + w_{dq}^2 - 1\right)w_{dq}$$
$$\dot{w}_q = c_q\left(Q - Q^{ref}\right)w_{qq}^2 \tag{8}$$
$$\dot{w}_{qq} = -\frac{c_qw_{qq}}{\Delta w_m^2}\left(Q-Q^{ref}\right)(w_q-w_m) - k\left(\frac{(w_q-w_m)^2}{\Delta w_m^2} + w_{qq}^2 - 1\right)w_{qq}.$$

Here $w_m = \frac{w_{max}+w_{min}}{2}$, $\Delta w_m = \frac{w_{max}-w_{min}}{2}$, c_d, c_q and k are positive constants. Note that w_{dq} and w_{qq} represent additional controller states that are required for the stability analysis of the system, as it is analyzed in the sequel using the Lyapunov theory. The complete implementation diagram of the proposed controller is shown in Fig. 3. The initial conditions of the controller states are defined as $w_{d0} = w_{q0} = w_m$, $w_{dq0} = w_{qq0} = 1$. It should be noted that the proposed method is significantly different from existing techniques that apply a virtual impedance since the controller dynamics are embedded inside the virtual resistances w_d and w_q.

The w_d dynamics (7) are investigated at first by considering the Lyapunov function candidate

$$W_d = \frac{(w_d - w_m)^2}{\Delta w_m^2} + w_{dq}^2. \tag{9}$$

Taking the time derivative of (9) with the consideration of $\dot{w}_d$

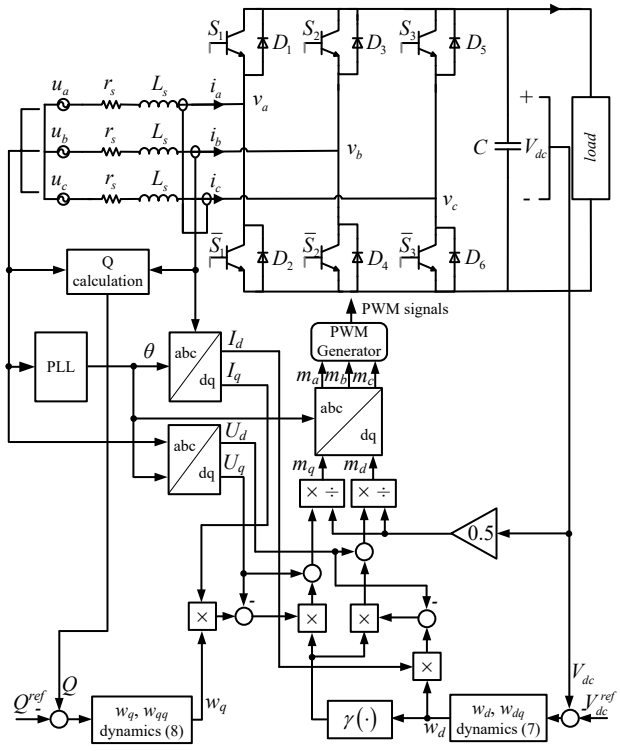

Fig. 3. Current-limiting controller for a three-phase rectifier

and $\dot{w}_{dq}$ from the dynamics (7), there is

$$\begin{aligned}\dot{W}_d &= \frac{2\left(w_d - w_m\right)\dot{w}_d}{\Delta w_m^2} + 2w_{dq}\dot{w}_{dq} \\ &= \frac{2\left(w_d - w_m\right)c_d\left(V_{dc} - V_{dc}^{ref}\right)w_{dq}^2}{\Delta w_m^2} \\ &- \frac{2(w_d - w_m)c_d\left(V_{dc} - V_{dc}^{ref}\right)w_{dq}^2}{\Delta w_m^2} - 2k\left(\frac{(w_d - w_m)^2}{\Delta w_m^2} + w_{dq}^2 - 1\right)w_{dq}^2 \\ &= -2k\left(\frac{(w_d - w_m)^2}{\Delta w_m^2} + w_{dq}^2 - 1\right)w_{dq}^2.\end{aligned}$$

This clearly shows that $\dot{W}_d$ is 0 on the ellipse

$$W_0 = \left\{ w_d, w_{dq} \in R : \frac{(w_d - w_m)^2}{\Delta w_m^2} + w_{dq}^2 = 1 \right\}$$

and on the axis $w_{dq} = 0$, positive inside the ellipse and negative outside of the ellipse. This means that starting with any initial conditions on the ellipse W_0, e.g. $w_{d0} = w_{q0} = w_m$, $w_{dq0} = w_{qq0} = 1$, the controller states w_d and w_{dq} always stay on W_0 for $t \geq 0$, as illustrated in Fig. 4(a). Hence, it is guaranteed that $w_d \in [w_{min}, w_{max}] = [w_m - \Delta w_m, w_m + \Delta w_m]$, $\forall t \geq 0$. By choosing the controller parameters $w_m > \Delta w_m > 0$, it is guaranteed that $w_{max} \geq w_d \geq w_{min} > 0$, $\forall t \geq 0$. As a consequence, it also holds that $\gamma(w_d) \in [0, 1]$.

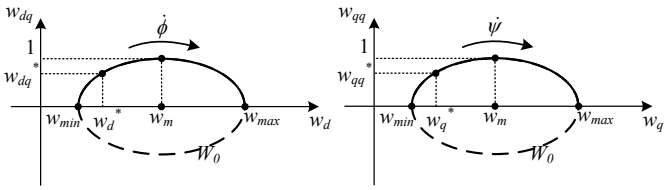

(a) $w_d - w_{dq}$ (b) $w_q - w_{qq}$

Fig. 4. Phase portrait of the controller dynamics

Using the transformation $w_d = w_m + \Delta w_m \sin\phi$, $w_{dq} = \cos\phi$, then from (7), there is

$$\dot{\phi} = \frac{c_d w_{dq}\left(V_{dc} - V_{dc}^{ref}\right)}{\Delta w_m}, \tag{10}$$

which shows that w_d and w_{dq} move on the ellipse W_0 with the angular velocity given by (10). Therefore, if V_{dc} approaches V_{dc}^{ref} then $\dot{\phi} \to 0$, which means w_d and w_{dq} stop moving and converge to the desired equilibrium, i.e. the proposed controller is capable of regulating the dc output voltage.

Note that starting from point $(w_m, 1)$, the controller states w_d and w_{dq} only move on the upper semi-ellipse of W_0 without moving around the ellipse because if the states try to reach the horizontal axis, i.e. $w_{dq} \to 0$, then $\dot{\phi} \to 0$ according to (10) and the controller states smoothly slow down independently from the difference $V_{dc} - V_{dc}^{ref}$. This prevents the states from crossing the horizontal axis and avoids a possible continuous oscillation for the controller dynamics.

Similarly, w_q and w_{qq} move on the same ellipse W_0, which results in $w_q \in [w_{min}, w_{max}] = [w_m - \Delta w_m, w_m + \Delta w_m] > 0, \forall t \geq 0$ with the same properties and the angular velocity $\dot{\psi} = \frac{c_q w_{qq}\left(Q - Q^{ref}\right)}{\Delta w_m}$, as shown in Fig. 4(b). Therefore, the reactive power regulation can be also achieved.

B. Closed-loop system stability

Since the initial conditions of the controller states are defined on the ellipse W_0 and $w_m > \Delta w_m > 0$, then $w_d, w_q \in [w_{min}, w_{max}] = [w_m - \Delta w_m, w_m + \Delta w_m] > 0, \forall t \geq 0$ and also $\gamma(w_d) \in [0, 1]$. By incorporating the controller (5)-(8) into the original plant (3), the current I_d and I_q dynamics can be investigated with respect to the varying w_d and w_q as

$$L_s\frac{dI_d}{dt} = -(r_s + \gamma(w_d)w_d)I_d - \omega L_s I_q + \gamma(w_d)U_d \tag{11}$$

$$L_s\frac{dI_q}{dt} = -(r_s + \gamma(w_d)w_q)I_q + \omega L_s I_d + \gamma(w_d)U_q, \tag{12}$$

while the dc output voltage dynamic equation becomes

$$C\frac{dV_{dc}}{dt} = \frac{P_o}{V_{dc}} - \frac{V_{dc}}{R_L}, \tag{13}$$

where $P_o = \frac{3}{2}\left[\gamma(w_d)\left(w_d I_d^2 + w_q I_q^2\right) + (1 - \gamma(w_d))(U_d I_d + U_q I_q)\right]$. Fig. 5 shows the equivalent circuit of the closed-loop system.

For system (11)-(12), consider the Lyapunov function candidate

$$V = \frac{1}{2}L_s I_d^2 + \frac{1}{2}L_s I_q^2.$$

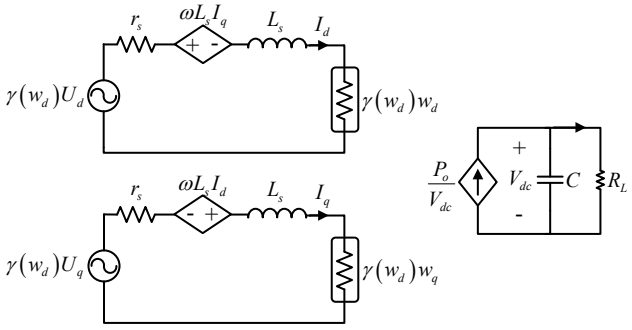

Fig. 5. Equivalent circuit of the closed-loop system

After taking into account (11)-(12), $w_d, w_q \in [w_{min}, w_{max}] > 0$ and $\gamma(w_d) \in [0, 1]$, its time derivative becomes

$$\begin{aligned}\dot{V} &= -(r_s + \gamma(w_d)w_d)I_d^2 - (r_s + \gamma(w_d)w_q)I_q^2 \\ &\quad + \gamma(w_d)U_d I_d + \gamma(w_d)U_q I_q \\ &\leq -(r_s + \gamma(w_d)w_{min})\left(I_d^2 + I_q^2\right) \\ &\quad + \gamma(w_d)\begin{bmatrix} U_d & U_q \end{bmatrix}\begin{bmatrix} I_d \\ I_q \end{bmatrix} \\ &\leq -(r_s + \gamma(w_d)w_{min})\left\|I\right\|_2^2 + \gamma(w_d)\left\|U\right\|_2\left\|I\right\|_2, \end{aligned} \quad (14)$$

where $I = \begin{bmatrix} I_d & I_q \end{bmatrix}^T$ and $U = \begin{bmatrix} U_d & U_q \end{bmatrix}^T$. Hence

$$\dot{V} < 0, \forall \|I\|_2 > \frac{\gamma(w_d)\left\|U\right\|_2}{r_s + \gamma(w_d)w_{min}}, \quad (15)$$

which means that system (11)-(12) is input-to-state stable (ISS) [35] with respect to the grid voltage vector U. Since for a balanced and stiff grid the values of U_d and U_q are bounded, the d and q currents I_d and I_q remain bounded for all $t \geq 0$ as well.

Additionally, as shown in the previous subsection, all controller states w_d, w_{dq}, w_q, w_{qq} are bounded as well since they are restricted on a given ellipse W_0. Therefore, the remaining dynamics of the dc side (13) can be rewritten as

$$\frac{1}{2}\frac{d\left(V_{dc}\right)^2}{dt} = -\frac{V_{dc}^2}{R_L} + P_o, \quad (16)$$

Note that system (16) can be seen as a linear time-invariant system with state V_{dc}^2 and input P_o, which is obviously bounded-input bounded-state stable. Since w_d, w_q are bounded and also I_d and I_q are bounded from the ISS property (15), then P_o is bounded. Therefore V_{dc}^2, and consequently V_{dc}, is bounded. As a result, the closed-loop system solution $(I_d(t), I_q(t), V_{dc}(t), w_d(t), w_{dq}(t), w_q(t), w_{qq}(t))$ is bounded for all $t \geq 0$.

Moreover, since $I = \begin{bmatrix} I_d & I_q \end{bmatrix}^T$, $U = \begin{bmatrix} U_d & U_q \end{bmatrix}^T$, then taking into account the dq transformation, it results in

$$\left\|I\right\|_2 = \sqrt{I_d^2 + I_q^2} = \sqrt{\left(\sqrt{2}I_{rms}\right)^2} = \sqrt{2}I_{rms}, \quad (17)$$

$$\left\|U\right\|_2 = \sqrt{U_d^2 + U_q^2} = \sqrt{\left(\sqrt{2}U_{rms}\right)^2} = \sqrt{2}U_{rms}. \quad (18)$$

For

$$w_{min} = \frac{U_{rms}}{I_{rms}^{max}}, \quad (19)$$

it is proven from the ISS property (15) that if initially the current is below the maximum allowed RMS value I_{rms}^{max}, i.e. $I_{rms}(0) < I_{rms}^{max}$, then

$$I_{rms}(t) \leq \frac{\gamma(w_d)U_{rms}}{r_s + \gamma(w_d)w_{min}} = \frac{I_{rms}^{max}}{\frac{r_s I_{rms}^{max}}{U_{rms}\gamma(w_d)} + 1} < I_{rms}^{max}, \forall t > 0, \quad (20)$$

Hence, the input current of the rectifier is always limited below I_{rms}^{max} with the appropriate choice of w_{min} given in (19) and the rectifier is protected at all times. By maintaining a lower limit for w_d and w_q from the proposed dynamics (7)-(8), both the closed-loop system stability and the desired current-limiting property are achieved. Since the dynamics (7)-(8) are analyzed using the Lyapunov theory, the required bounds for w_d and w_q are guaranteed without applying additional saturation units. In addition, the proposed controller slows down the integration near the limits and therefore it does not suffer from integrator windup issues, which may lead to instability. This is a crucial property that distinguishes the proposed controller with traditional current-limiting approaches that incorporate current saturation units.

Since the ellipse W_0 is a closed curve and the selection of w_{min} corresponds to the maximum current I_{rms}^{max}, the selection of w_{max} corresponds to a minimum input current I_{rms}^{min}, i.e.

$$w_{max} = \frac{U_{rms}}{I_{rms}^{min}}. \quad (21)$$

Note that since the controller should be able to operate the system for the cases of large values of the load R_L or even without a load connected to the rectifier output, i.e. $R_L = \infty$, then I_{rms}^{min} can be chosen arbitrarily small (around mA or μA) to cover the parasitic losses of the switching elements, the inductors and the capacitor.

It is noted that when $I_{rms} \to I_{rms}^{max}$ then $w_d \to 0$ or $w_q \to 0$. This means that $w_{dq} \to 0$ or $w_{qq} \to 0$ and from (7)-(8) it results in $\dot{w}_d \to 0$ or $\dot{w}_q \to 0$, respectively. This means that the integration slows down. Additionally, the controller remains as a continuous-time system, which facilitates the stability analysis.

Since $I_{rms} < I_{rms}^{max}$ holds true and the grid voltage is stiff, i.e. U_{rms} is constant, then the proposed controller guarantees a given bound at the apparent power

$$S < S^{max}, \quad (22)$$

where $S = 3U_{rms}I_{rms}$ and $S^{max} = 3U_{rms}I_{rms}^{max}$. By neglecting the small resistance r_s of the filter inductors and the rectifier losses, then from the power balance between the ac and the dc sides, at the steady state, there is

$$\frac{\left(V_{dc}^e\right)^2}{R_L} < 3U_{rms}I_{rms}^{max}.$$

Taking into account that $V_{dc} \geq 2\sqrt{2}U_{rms}$ for linear modulation and sinusoidal PWM operation [36], then a minimum value of the resistive load can be obtained as

$$R_L > \frac{8U_{rms}}{3I_{rms}^{max}}. \quad (23)$$

This inequality makes sense since for a smaller resistance, the input current cannot be limited below I_{rms}^{max} with any controller

due to the boost function of the rectifier where the current can flow through the diodes.

Finally, since a limitation in the apparent power is guaranteed from (22), when the current reaches the limit and the output voltage converges to $V_{dc}^{e} \neq V_{dc}^{ref}$, the reactive power would be regulated to

$$Q^{e} = \pm\sqrt{(S^{max})^2 - (P^{e})^2} = \pm\sqrt{9U_{rms}^2 (I_{rms}^{max})^2 - \frac{(V_{dc}^{e})^4}{R_L^2}}. \quad (24)$$

As a result, if $\left|Q^{ref}\right| > |Q^{e}|$, then the reactive power converges to Q^{e} in order for the rectifier to guarantee the current limitation. In other words, the proposed controller is able to limit the current and consequently the apparent power automatically without modifying the control structure.

It becomes clear from (15) and (20) that the RMS value of the rectifier current is limited below a value related to $\|U\|_2 = \sqrt{U_d^2 + U_q^2}$, which is equal to the RMS value of the grid voltage U_{rms}. If the grid is weak or subject to voltage variations, the same analysis holds true and guarantees that I_{rms} is limited below $\frac{\gamma(w_d)\max\{U_{rms}\}}{r_s+\gamma(w_d)w_{min}}$. Hence, based on the expression in (19), w_{min} can be selected as $\frac{\max\{U_{rms}\}}{I_{rms}^{max}}$ and (20) becomes

$$\begin{aligned} I_{rms}(t) &\leq \frac{\gamma(w_d)U_{rms}}{r_s + \gamma(w_d)w_{min}} = \frac{\frac{U_{rms}}{\max\{U_{rms}\}} I_{rms}^{max}}{\frac{r_s I_{rms}^{max}}{\max\{U_{rms}\}\gamma(w_d)} + 1} \\ &< \frac{1}{\frac{r_s I_{rms}^{max}}{\max\{U_{rms}\}\gamma(w_d)} + 1} I_{rms}^{max} < I_{rms}^{max}, \ \forall t > 0, \quad (25) \end{aligned}$$

Hence, given a maximum value $\max\{U_{rms}\}$ and the choice of w_{min}, the stability and the current-limiting property of the rectifier can be guaranteed.

C. Operation when the load is disconnected

One of the crucial properties that a three-phase rectifier should guarantee is to avoid instability when the load is disconnected from the rectifier (transition to no load operation). Considering the steady-state condition where $V_{dc} = V_{dc}^{ref}$ corresponding to the currents I_d^e and I_q^e, then when suddenly the load is disconnected, the output voltage V_{dc} starts increasing due to the existing dq currents. In this case, $V_{dc} - V_{dc}^{ref} > 0$ and from (10) the controller states w_d and w_{qd} move clockwise on the ellipse W_0 leading to $w_d \to w_{max}$. Consequently, $\gamma(w_d) = 0$ when $w_d = w_{max}$ and (5), (6) become

$$m_d = \frac{2U_d}{V_{dc}}, \ m_q = \frac{2U_q}{V_{dc}},$$

which makes the rectifier voltages equal to the grid voltages, i.e. $V_d = U_d$ and $V_q = U_q$. Hence, both currents I_d and I_q become zero and the rectifier stops charging the output capacitor, thus avoiding the output voltage to further increase. In practice, during this operation, the capacitor is discharged through the parasitic elements of the rectifier and the capacitor. When the load is reconnected, then the controller returns to its normal operation. This will be verified further in the results shown in Section V.

The voltage V_{dc} may increase too much but this can be easily addressed because most rectifiers are equipped with over-voltage protection in practice [37]. In addition, due to the very small values of the parasitic elements, it might take a long time for the capacitor to discharge. In such cases, choppers can be added to consume part of the stored energy that is injected into the rectifier during the transient.

D. Selecting the controller parameters

The controller parameters w_{min} and w_{max} can be selected according to (19) and (21), respectively. Since these values represent the limits of w_d and w_q which operate on the ellipse W_0, as shown in Fig. 4, the controller parameters w_m and Δw_m, which corresponds to the center of the ellipse and the horizontal radius, respectively, are given as

$$w_m = \frac{w_{max} + w_{min}}{2} = \frac{U_{rms}}{2}\left(\frac{1}{I_{rms}^{min}} + \frac{1}{I_{rms}^{max}}\right), \quad (26)$$

$$\Delta w_m = \frac{w_{max} - w_{min}}{2} = \frac{U_{rms}}{2}\left(\frac{1}{I_{rms}^{min}} - \frac{1}{I_{rms}^{max}}\right). \quad (27)$$

Additionally, the gain k is arbitrarily selected as a positive constant since it is multiplied with the terms $\frac{(w_d - w_m)^2}{\Delta w_m^2} + w_{dq}^2 - 1$ and $\frac{(w_q - w_m)^2}{\Delta w_m^2} + w_{qq}^2 - 1$, which are zero on W_0. In fact, k is only used for the practical implementation to increase the robustness of the w_{dq} and w_{qq} dynamics with respect to numerical and computational errors. Hence, in practice if w_{dq} and w_{qq} are disturbed from the desired ellipse W_0, the positive gain k will force them to be attracted again on it. A typical range for k is $[1, 1000]$.

Parameters c_d and c_q are found inside the angular velocity expressions $\dot{\phi}$, $\dot{\psi}$ and affect the dynamic performance. Since w_d and w_{dq} are restricted on the upper semi-ellipse of W_0, the worst-case scenario is when w_d starts from w_{max} and reaches the minimum value w_{min} at the steady state. In this case, the dc output voltage starts from a minimum value V_{dc}^{init} and reaches V_{dc}^{e}, corresponding to the maximum input current I_{rms}^{max}, i.e. there is a maximum difference $\Delta V_{dc}^{max} = \left|V_{dc}^{e} - V_{dc}^{init}\right|$. Assuming that t_s is the settling time for the plant in order for w to travel on the upper semi-ellipse of W_0, which corresponds to an arc with central angle $\pi\, rad$, then in the worst-case scenario the angular velocity is constant and equal to its maximum value $\dot{\phi}_{max} = \frac{\pi}{t_s}\, rad/s$. Since $w_q \leq 1$ on the upper semi-ellipse of W_0:

$$\dot{\phi} < \dot{\phi}_{max} = \frac{c_d \Delta V_{dc}^{max}}{\Delta w_m} = \frac{\pi}{t_s}$$

i.e.

$$c_d = \frac{\pi \Delta w_m}{t_s \Delta V_{dc}^{max}}. \quad (28)$$

Similarly, c_q can be calculated as

$$c_q = \frac{\pi \Delta w_m}{t_s \Delta Q^{max}}, \quad (29)$$

for a given maximum deviation of the reactive power ΔQ^{max}. For systems with fast dynamics, the values of c_d and c_q can be significantly increased. Expressions (28) and (29) are obtained from the worst-case scenario to provide some starting values for the control parameters c_d and c_q, respectively.

Finally, the alignment angle θ_α for the generic $\alpha\beta$ transformation. If $\theta_\alpha = 0$ or $\theta_\alpha = 90^o$, then U_q or U_d is zero. In

this case, for a typical unity power factor application, I_d or I_q should be regulated to zero which implies from (5)-(6) that m_d or m_q is zero independently from the controller dynamics w_d or w_q. Hence, for the desired operation, it is required that $0 < \theta_\alpha < 90^o$, which leads to $I_d,\, I_q > 0, \forall t \geq 0$, since $V_d,\, V_q \geq 0$ results from $U_d,\, U_q > 0$ when ignoring the voltage drop on the filter inductor and $w_d,\, w_q > 0$. By ignoring the negligible parasitic resistance of the filter inductors, then at the steady state it yields from (4) that

$$I_d^e = \frac{U_d \left(V_{dc}^e\right)^2}{3U_{rms}^2 R_L} - \frac{U_q Q^e}{3U_{rms}^2},\; I_q^e = \frac{U_q \left(V_{dc}^e\right)^2}{3U_{rms}^2 R_L} + \frac{U_d Q^e}{3U_{rms}^2}. \quad (30)$$

For $I_d^e,\, I_q^e > 0$, (30) provides that

$$-\frac{U_q \left(V_{dc}^e\right)^2}{U_d R_L} < Q^e < \frac{U_d \left(V_{dc}^e\right)^2}{U_q R_L}. \quad (31)$$

If the a axis is oriented very close to the α axis, i.e., $\theta_\alpha \approx 0$, then $U_q \approx 0$ and the reactive power is restricted to positive values from (31); if it is oriented close to the β axis, i.e. $\theta_\alpha \approx 90^o$, then the reactive power is restricted to negative values. As a result, in order to have the flexibility of controlling the reactive power in either positive or negative values even when the current is limited, the orientation should be selected somewhere between the two vertical axes α and β. It is therefore convenient to chose the orientation exactly in the middle of the two axes, i.e. $\theta_\alpha = 45^o$. In this case, the reactive power can be controlled within the range of

$$-\frac{\left(V_{dc}^e\right)^2}{R_L} < Q^e < \frac{\left(V_{dc}^e\right)^2}{R_L}, \quad \text{or} \quad -P^e < Q^e < P^e. \quad (32)$$

It is underlined that the controller equations (7)-(8) are not affected by the choice of θ_α since they require the calculation of the reactive power Q which will be the same independently from the $\alpha\beta$ transformation and the virtual resistances w_d and w_q will remain bounded in a positive set to guarantee the desired stability and current limitation.

IV. The case with an LCL filter

The boosting inductance L_s in each phase operates as a low-pass filter to reduce the high-frequency of the input current i, caused by the switching operation of the three-phase rectifier. However, in many rectifiers, an LCL filter is often used to achieve better harmonic rejection. Denote the d and q axis components of the capacitor voltage of the LCL filter as V_{cd} and V_{cq}. Then, the rectifier current equations become similarly to (3) as

$$L_s \frac{dI_d}{dt} = -r_s I_d - \omega L_s I_q - m_d \frac{V_{dc}}{2} + V_{cd} \quad (33)$$

$$L_s \frac{dI_q}{dt} = -r_s I_q + \omega L_s I_d - m_q \frac{V_{dc}}{2} + V_{cq}. \quad (34)$$

In order to guarantee the current-limiting property of the rectifier, the proposed controller (5)-(6) can be modified as

$$m_d = \frac{2}{V_{dc}} \left(\gamma(w_d) \left(w_d I_d - U_d\right) + V_{cd}\right) \quad (35)$$

$$m_q = \frac{2}{V_{dc}} \left(\gamma(w_d) \left(w_q I_q - U_q\right) + V_{cq}\right), \quad (36)$$

while the controller equations (7)-(8) will remain the same. In this case, by substituting (35)-(36) into (33)-(34), the closed-loop system equations become the same as (11)-(12), which means that the same analysis given in Section III holds and the RMS value of the rectifier current is limited below I_{rms}^{max}.

V. Validation via real-time simulations

A. With a resistive load

In order to verify the proposed current-limiting nonlinear controller, a three-phase rectifier feeding a resistive load with parameters given in Table I is tested using an OPAL-RT real-time digital simulator with the actual switching model of the rectifier in real time with the step size of 8 μs. Ideally, the smaller step size the better but it is limited by the hardware. Nevertheless, the real-time simulations are conducted to verify the performance of the proposed controller in real-time, as it could have been implemented in a hardware rectifier, compared to other simulation environments (e.g. Matlab, Simulink, PLECS). Since the main application of a rectifier is to maintain a constant dc output voltage, the reference of the dc output voltage is set to $V_{dc}^{ref} = 300\,\text{V}$ for the entire test. At the time instant $t = 0.1\,\text{s}$, while the load R_L is $200\,\Omega$, the desired reactive power is changed from 0 to $Q^{ref} = 100\,\text{Var}$ and then returned to zero after $0.4\,\text{s}$. At $t = 0.9\,\text{s}$, the load R_L is changed to $100\,\Omega$. In order to verify the current-limiting property of the controller, at $t = 1.3\,\text{s}$, the load resistance is decreased further to $50\,\Omega$ and then back to $100\,\Omega$ after $0.4\,\text{s}$.

Fig. 6 illustrates the performance of the rectifier under the given scenario. During the first $1.3\,\text{s}$, the dc output voltage and the reactive power are regulated at their desired values, even after the rapid change of the load or the reactive power reference. The transient response of the d and q components of the input current and the controller states is shown in Fig. 6(b). At the time instant $t = 1.3\,\text{s}$, when the load is decreased to $50\,\Omega$, which leads to a high input current, it can be seen that the dc output voltage is regulated to a value slightly lower than the reference since the RMS input current increases to nearly the limit I_{rms}^{max}. This is clearly shown in Fig. 6(a), where the RMS value of the current is regulated to a value slightly less than the maximum limit $I_{rms}^{max} = 6\,\text{A}$, due to presence of the small parasitic resistance r_s. Hence, $I_{rms} < I_{rms}^{max}$ is maintained at all times, which verifies the current-limiting property. When the load returns to $100\,\Omega$ at $t = 1.7\,\text{s}$, the dc output voltage returns to its reference value after a transient. The slow response is due to the slow action of the controller

TABLE I
RECTIFIER AND CONTROLLER PARAMETERS

Parameters	Values	Parameters	Values
L_s	$2.2\,\text{mH}$	switching frequency	$10\,\text{kHz}$
r_s	$0.5\,\Omega$	I_{rms}^{max}	$6\,\text{A}$
C	$300\,\mu\text{F}$	I_{rms}^{min}	$10\,\text{mA}$
R_L	$50 \sim 200\,\Omega$	k	1000
V_{rms}	$100\,\text{V}$	t_s	$0.01\,\text{s}$
ω	100π rad/s	ΔV_{dc}^{max}	$200\,\text{V}$
θ_α	45^o	ΔQ^{max}	$200\,\text{Var}$

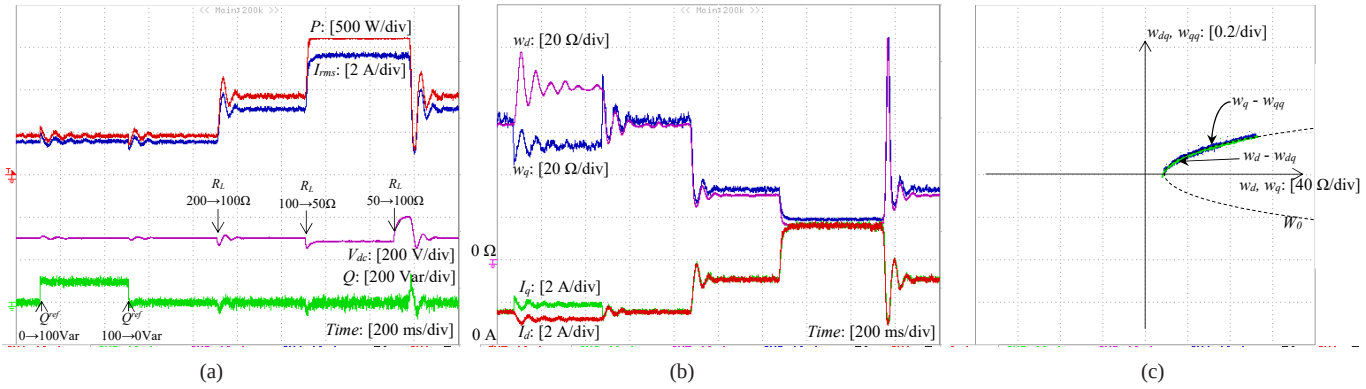

Fig. 6. Transient response of the three-phase rectifier with a linear load: (a) real power P, reactive power Q, output voltage V_{dc} and RMS input current I_{rms}, (b) d and q components of the input current (I_d, I_q) and the controller states w_d and w_q, and (c) phase portrait of the controller dynamics

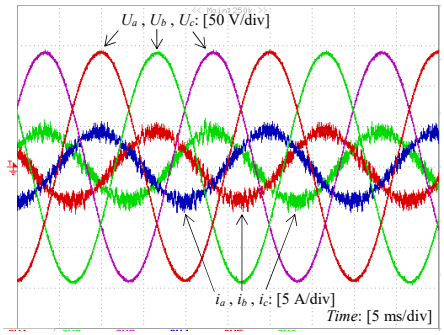

Fig. 7. Steady-state response of the three-phase rectifier with a linear load

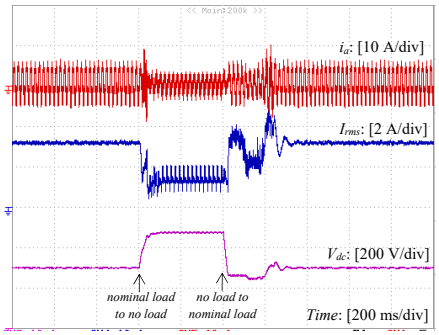

Fig. 8. Time response of the three-phase rectifier when the linear load is changed from the nominal load to no load and back

which mainly depends on the selection of the gains c_d and c_q. Further improvement of the transient response is a very interesting topic and will be examined in future work, since the main purpose of this paper is to introduce for the first time the current-limiting structure of the proposed controller. Since $\theta_\alpha = 45^o$ for the $\alpha\beta$ transformation, then $U_d = U_q = U_{rms}$ and therefore from (4), when the reactive power is set to zero it results in $I_d = I_q = I_{rms}$. This is clearly depicted in Fig. 6(b), where $I_d = I_q$ when $Q = 0\,\text{Var}$, as required by the unity power factor. Fig. 6(c) illustrates the phase portrait of the controller states w_d, w_{dq} and w_q, w_{qq}, respectively, where the theoretical analysis is verified since the controller states remain on the upper semi-ellipse of W_0 until they converge to the corresponding equilibrium points. The steady-state response of the system is shown in Fig. 7. The switching ripples are visible in the current waveforms, although some additional noise is added due to the limitation of the OPAL-RT system with respect to the minimum time step required in order to obtain the results in real time.

In order to further validate the effectiveness of the proposed controller, while the load resistance is at its nominal value $R_L = 100\,\Omega$, the entire load is suddenly disconnected to investigate the transition to the no-load condition. The response of the rectifier is shown in Fig. 8. It can be seen, that the output voltage increases for a very short time, during which the controller states w_d and w_q converge to the maximum value w_{max}, as discussed in Subsection III-C. Then both currents I_d and I_q become zero and stop charging the capacitor. This is clear from Fig. 8 where the instantaneous current is quickly reduced to a very small value around zero, without noticeable fundamental components. The RMS value does not converge to zero due to the ripples in the current. However, it is clear that no current flows to the dc side since the capacitor voltage does not increase any further. After this operation, in practice, the capacitor is slowly discharged through the parasitic elements of the rectifier components. The over-voltage does not cause any problem to the load but this should be taken into consideration when selecting the devices. If needed, a simple over-voltage protection circuit can be added to limit the voltage increase. It should be highlighted that the faster the controller dynamics, i.e. for large c_d and c_q, the lower the dc output voltage increase, since both w_d and w_q converge faster to its maximum value w_{max}. However, this can lead to a more

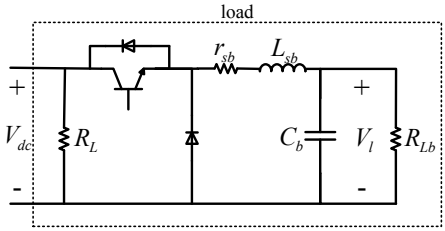

Fig. 9. DC-DC buck converter load

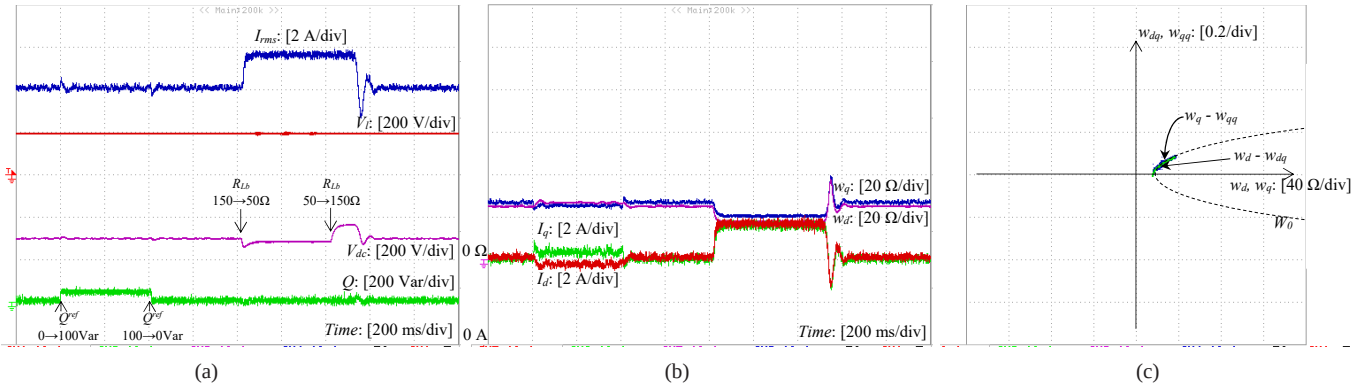

Fig. 10. Transient response of the three-phase rectifier with a dc/dc buck converter load: (a) load voltage V_l, reactive power Q, output voltage V_{dc} and RMS input current I_{rms}, (b) d and q components of the input current (I_d, I_q) and the controller states w_d, w_q and (c) phase portrait of the controller dynamics

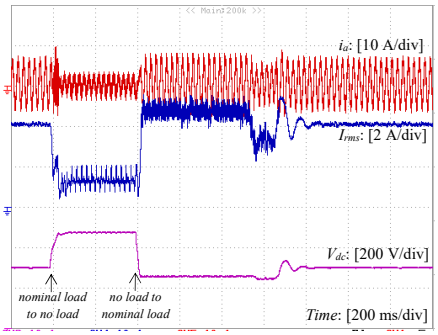

Fig. 11. Time response of the three-phase rectifier when the dc/dc buck converter load is changed from the nominal load to no load and back

oscillatory response under normal operation. This provides useful insights to further enhance the transient response of the controller in the future. When the nominal load is reconnected to the device after almost $0.1\,$s, the proposed controller leads the output voltage to its reference value after a short transient, as shown in Fig. 8.

B. With a converter-fed load

Since in modern smart grid applications, more complicated loads are often used, here, a dc/dc buck converter connected to the output of the rectifier in parallel with the resistive load, as shown in Fig. 9, is tested. The buck converter is controlled using a traditional PI controller to regulate the output voltage V_l at $200\,$V. The parameters of the load converter are $L_{sb} = 2.2\,$mH, $r_{sb} = 0.5\,\Omega$, $C_b = 300\mu F$ and $R_{Lb} = 150\,\Omega$.

While the dc output voltage of the rectifier is regulated at $V_{dc}^{ref} = 300\,$V, the reactive power reference changes from 0 to $100\,$Var at $t = 0.2\,$s and returns to 0 after $0.4\,$s. As it is shown in Fig. 10(a), both the dc output voltage and the reactive power are regulated at their reference values, while the load voltage V_l is maintained at the desired value. At the time instant $t = 1\,$s, the load R_{Lb} of the buck converter is changed from $150\,\Omega$ to $50\,\Omega$, which increases the injected power, since the voltage of the load is maintained constant, and consequently the rectifier current. However, since the proposed controller guarantees a current-limiting property, the current I_{rms} approaches its maximum value and the dc output voltage of the rectifier slightly drops to maintain the maximum power of the device. In this way, the rectifier is protected at all times, which is the main goal of the proposed controller, while the load voltage is maintained at its reference value. The load of the buck converter returns to its original value $0.4\,$s later. The time response of the rectifier currents and the controller states are shown in Fig. 10(b). Note that due to the buck converter dynamics and the PI controller used, the desired load voltage V_l remains constant with almost no visible variations for the entire operation. The controller states w_d,w_{dq} and w_q, w_{qq} operate once again exclusively on the ellipse W_0, as illustrated in Fig. 10(c), verifying the theory developed in the paper.

The operation of the rectifier under a sudden disconnection and reconnection of the load (transition from nominal-load to no-load conditions and vice versa) is shown in Fig. 11. It is observed that the current limitation is maintained at all times. The slower response of the rectifier during the reconnection of the load compared to the case of the linear load (Fig. 8) is due to the buck converter dynamics and the PI controller used for the regulation of the load voltage.

VI. Conclusions

A nonlinear controller to inherently limit the current drawn from the grid by a three-phase rectifier has been proposed, in addition to achieving accurate output voltage regulation and reactive power control, using the nonlinear model dynamics and the generic dq transformation. The current-limiting property of the proposed controller does not depend on the system parameters and is maintained for both linear and nonlinear loads used in smart grid applications. An analytic framework for selecting the controller parameters has been presented and a small modification of the controller is also proposed to guarantee the desired current limitation in the LCL filter case. The desired performance has been extensively tested using a real-time simulation system with different types of loads.

However, it is clear from (25) that $I_{rms}(t) < \frac{U_{rms}}{\max\{U_{rms}\}} I_{rms}^{max}$ which means that the maximum value of the current will be below I_{rms}^{max} as required but drop when U_{rms} drops. Further research is required to maximize the current capability of the three-phase current-limiting rectifiers in order

to support the grid under faults, i.e. by injecting a higher value of reactive power as imposed by the Grid Codes. Future research will also include the experimental implementation of the proposed technique under different types of loads (e.g. constant current, constant power), the improvement of the transient response and the complete investigation of the system nonlinearities, including internal clock delays, modulation, etc.

REFERENCES

[1] Q.-C. Zhong and T. Hornik, *Control of Power Inverters in Renewable Energy and Smart Grid Integration*. Wiley-IEEE Press, 2013.

[2] R. Majumder, "A hybrid microgrid with DC connection at back to back converters," *IEEE Transactions on Smart Grid*, vol. 5, no. 1, pp. 251–259, 2014.

[3] N. Zhou, J. Wang, Q. Wang, and N. Wei, "Measurement-based harmonic modeling of an electric vehicle charging station using a three-phase uncontrolled rectifier," *IEEE Transactions on Smart Grid*, vol. 6, no. 3, pp. 1332–1340, 2015.

[4] A. Dubey, S. Santoso, and M. P. Cloud, "Average-value model of electric vehicle chargers," *IEEE Transactions on Smart Grid*, vol. 4, no. 3, pp. 1549–1557, 2013.

[5] M. Parvez Akter, S. Mekhilef, N. Mei Lin Tan, and H. Akagi, "Modified model predictive control of a bidirectional AC-DC converter based on lyapunov function for energy storage systems," *IEEE Trans. Ind. Electron.*, vol. 63, no. 2, pp. 704–715, Feb. 2016.

[6] P. R. Martinez-Rodriguez, G. Escobar, A. A. Valdez-Fernandez, M. Hernandez-Gomez, and J. M. Sosa, "Direct power control of a three-phase rectifier based on positive sequence detection," *IEEE Trans. Ind. Electron.*, vol. 61, no. 8, pp. 4084–4092, Aug. 2014.

[7] V. Blasko and V. Kaura, "A new mathematical model and control of a three-phase AC-DC voltage source converter," *IEEE Trans. Power Electron.*, vol. 12, no. 1, pp. 116–123, 1997.

[8] J. Dannehl, C. Wessels, and F. W. Fuchs, "Limitations of voltage-oriented PI current control of grid-connected PWM rectifiers with LCL filters," *IEEE Trans. Ind. Electron.*, vol. 56, no. 2, pp. 380–388, Feb. 2009.

[9] A. Yazdani and R. Iravani, *Voltage-Sourced Converters in Power Systems: Modeling, Control, and Applications*. John Wiley & Sons, Inc., 2010.

[10] J. P. Contreras and J. M. Ramirez, "Multi-fed power electronic transformer for use in modern distribution systems," *IEEE Transactions on Smart Grid*, vol. 5, no. 3, pp. 1532–1541, 2014.

[11] M. Malinowski, M. P. Kazmierkowski, S. Hansen, F. Blaabjerg, and G. D. Marques, "Virtual-flux-based direct power control of three-phase PWM rectifiers," *IEEE Trans. Ind. Appl.*, vol. 37, no. 4, pp. 1019–1027, 2001.

[12] J. G. Norniella, J. M. Cano, G. A. Orcajo, C. H. Rojas, J. F. Pedrayes, M. F. Cabanas, and M. G. Melero, "Improving the dynamics of virtual-flux-based control of three-phase active rectifiers," *IEEE Trans. Ind. Electron.*, vol. 61, no. 1, pp. 177–187, Jan. 2014.

[13] M. Liserre, A. Del'Aquila, and F. Blaabjerg, "Genetic algorithm-based design of the active damping for an LCL-filter three-phase active rectifier," *IEEE Trans. Power Electron.*, vol. 19, no. 1, pp. 76–86, 2004.

[14] L. Hang, S. Liu, G. Yan, B. Qu, and Z.-Y. Lu, "An Improved Deadbeat Scheme With Fuzzy Controller for the Grid-side Three-Phase PWM Boost Rectifier," *IEEE Trans. Power Electron.*, vol. 26, no. 4, pp. 1184–1191, 2011.

[15] S. Vazquez, J. A. Sanchez, J. M. Carrasco, J. I. Leon, and E. Galvan, "A Model-Based Direct Power Control for Three-Phase Power Converters," *IEEE Trans. Ind. Electron.*, vol. 55, no. 4, pp. 1647–1657, 2008.

[16] Y. Zhang, Z. Li, Y. Zhang, W. Xie, Z. Piao, and C. Hu, "Performance improvement of direct power control of PWM rectifier with simple calculation," *IEEE Trans. on Power Electron.*, vol. 28, no. 7, pp. 3428–3437, 2013.

[17] Y. Ye, M. Kazerani, and V. H. Quintana, "Modeling, control and implementation of three-phase PWM converters," *IEEE Trans. Power Electron.*, vol. 18, no. 3, pp. 857–864, 2003.

[18] X. Guo, Z. Lu, B. Wang, X. Sun, L. Wang, and J. M. Guerrero, "Dynamic phasors-based modeling and stability analysis of droop-controlled inverters for microgrid applications," *IEEE Trans. Smart Grid*, vol. 5, no. 6, pp. 2980–2987, 2014.

[19] T.-S. Lee, "Lagrangian modeling and passivity-based control of three-phase AC/DC voltage-source converters," *IEEE Transactions on Industrial Electronics*, vol. 51, no. 4, pp. 892–902, 2004.

[20] M. Perez, R. Ortega, and J. R. Espinoza, "Passivity-based PI control of switched power converters," *IEEE Trans. Control Syst. Technol.*, vol. 12, no. 6, pp. 881–890, 2004.

[21] A. Gensior, H. Sira-RamÃrez, J. Rudolph, and H. GÃ¼ldner, "On some nonlinear current controllers for three-phase boost rectifiers," *IEEE Trans. Industrial Electron.*, vol. 56, no. 2, pp. 360–370, 2009.

[22] J. R. Espinoza and G. Joos, "State variable decoupling and power flow control in PWM current-source rectifiers," *IEEE Trans. Ind. Electron.*, vol. 45, no. 1, pp. 78–87, 1998.

[23] D.-C. Lee, "Advanced nonlinear control of three-phase PWM rectifiers," *IEE Proceedings-Electric Power Applications*, vol. 147, no. 5, pp. 361–366, 2000.

[24] C. Wan, M. Huang, C. K. Tse, S.-C. Wong, and X. Ruan, "Nonlinear Behavior and Instability in a Three-Phase Boost Rectifier Connected to a Nonideal Power Grid With an Interacting Load," *IEEE Trans. Power Electron.*, vol. 28, no. 7, pp. 3255–3265, 2013.

[25] M. Huang, S.-C. Wong, C. K. Tse, and X. Ruan, "Catastrophic Bifurcation in Three-Phase Voltage-Source Converters," *IEEE Trans. Circuits Syst. I*, vol. 60, no. 4, pp. 1062–1071, 2013.

[26] G. C. Konstantopoulos and A. T. Alexandridis, "Design and analysis of a novel bounded nonlinear controller for three-phase ac/dc converters," in *52nd IEEE Annual Conference on Decision and Control (CDC)*, pp. 3659–3664, Firenze, Italy, Dec. 10-13 2013.

[27] K. F. Krommydas and A. T. Alexandridis, "Nonlinear stability analysis for ac/dc voltage source converters driven by PI current-mode controllers," in *Control Conference (ECC), 2014 European*, pp. 2774–2779, Strasbourg, France, June 24-27 2014.

[28] G. C. Konstantopoulos and Q.-C. Zhong, "Nonlinear control of single-phase PWM rectifiers with inherent current-limiting capability," *IEEE Access*, vol. 4, pp. 3578–3590, 2016.

[29] Q.-C. Zhong and G. C. Konstantopoulos, "Current-limiting droop control of grid-connected inverters," *IEEE Trans. Ind. Electron.*, 2017, to appear.

[30] N. Bottrell and T. C. Green, "Comparison of current-limiting strategies during fault ride-through of inverters to prevent latch-up and wind-up," *IEEE Trans. Power Electron.*, vol. 29, no. 7, pp. 3786–3797, 2014.

[31] A. D. Paquette and D. M. Divan, "Virtual impedance current limiting for inverters in microgrids with synchronous generators," *IEEE Trans. Ind. Appl.*, vol. 51, no. 2, pp. 1630–1638, 2015.

[32] L. Zaccarian and A. R. Teel, "Nonlinear scheduled anti-windup design for linear systems," *IEEE Trans. Autom. Control*, vol. 49, no. 11, pp. 2055–2061, 2004.

[33] S. Tarbouriech and M. Turner, "Anti-windup design: an overview of some recent advances and open problems," *IET Control Theory & Applications*, vol. 3, no. 1, pp. 1–19, 2009.

[34] G. C. Konstantopoulos, Q.-C. Zhong, B. Ren, and M. Krstic, "Bounded integral control of input-to-state practically stable nonlinear systems to guarantee closed-loop stability," *IEEE Trans. Autom. Control*, vol. 61, DOI 10.1109/TAC.2016.2552978, no. 12, pp. 4196–4202, Dec. 2016.

[35] H. K. Khalil, *Nonlinear Systems*. Prentice Hall, 2001.

[36] B. Bose, *Modern Power Electronics and AC Drives*. Englewood Cliffs, NJ: Prentice-Hall, 2001.

[37] Semiconductor Components Industries, LLC, "Transient overvoltage protection," Tech. Rep., Apr. 2008, available at http://www.onsemi.com.

Qing-Chang Zhong (M'03-SM'04-F'17) received the Ph.D. degree in control and power engineering from Imperial College London in 2004 and the Ph.D. degree in control theory and engineering from Shanghai Jiao Tong University in 2000. He holds the Max McGraw Endowed Chair Professor in Energy and Power Engineering at the Dept. of Electrical and Computer Engineering, Illinois Institute of Technology, USA. He is a Fellow of IEEE and IET, a Distinguished Lecturer of IEEE Power Electronics Society, IEEE Control Systems Society and IEEE Power and Energy Society, and the Vice-Chair of IFAC TC Power and Energy Systems. He was a Senior Research Fellow of Royal Academy of Engineering, UK, and the UK Representative to European Control Association. He serves/d as AE for IEEE TAC/TIE/TPELS/TCST/Access/JESTPE.

George C. Konstantopoulos (S'07-M'13) received his Diploma and Ph.D. degrees in electrical and computer engineering from the Department of Electrical and Computer Engineering, University of Patras, Rion, Greece, in 2008 and 2012, respectively. From 2011 to 2012, he was an Electrical Engineer with the Public Power Corporation of Greece. Since 2013, he has been with the Department of Automatic Control and Systems Engineering, The University of Sheffield, U.K., initially as a postdoctoral researcher and now as a Lecturer. Dr. Konstantopoulos is a Member of the National Technical Chamber of Greece.